Sensors and Materials, Vol. 36, No. 9 (2024) 3933–3946
MYU Tokyo

S & M 3776

Analysis of Relative Land Surface Temperature by Land Cover Using Landsat 8 Imagery: Focusing on Chuncheon City

Young-Jo Yun,[1] Sung-Ho Kil,[1*] and Sungmin Lee[2]

[1]Department of Landscape Architecture, Kangwon National University,
Gangwon-Dae-Hak-Gil 1, Chuncheon, Gangwondo 24341, Republic of Korea
[2]Department of Landscape Architecture and Urban Planning, Texas A&M University,
College Station, TX 77843-3137, United States of America

(Received July 25, 2024; accepted September 20, 2024)

Keywords: Landsat imagery, land surface temperature, remote sensing, urban heat island

In this study, we analyzed the surface temperature of Chuncheon from 2014 to 2020 using Landsat 8 images. The findings revealed that man-made structures such as asphalt roads and buildings cause significant increases in land surface temperatures in urbanized, arid, and residential areas. Industrial areas exhibited the highest relative land surface temperature (*RLST*) index, while densely populated residential areas showed relatively high *RLST* values. Conversely, areas with high-rise apartments had lower land surface temperatures due to shade and green space. Natural land cover areas demonstrated negative mean *RLST*, highlighting the usefulness of *RLST* in distinguishing temperature differences between land cover types. A 0 °C reference surface temperature was used in *RLST* to standardize land surface temperature measurements, which helped understand land cover status. As the urban heat island phenomenon continues, land surface temperatures are gradually rising. To build a sustainable urban ecosystem, policies and plans to expand and improve green spaces and waterfront environments are essential. To achieve these goals, a comprehensive strategy for expanding and improving green spaces is needed, as well as various policies to improve water quality.

1. Introduction

Various environmental changes caused by climate change are having severe impacts on ecosystems and resource management.(1) The Ministry of Environment(2) predicted that Earth's temperature will rise by approximately 1.9 to 5.2 ℃ from the current level depending on greenhouse gas emissions by the end of the 21st century. In particular, rapid urbanization around the world in recent decades has worsened the urban heat island phenomenon and caused various environmental problems.(3) These problems include changes in urban ecosystems and increased health risks for urban residents.(4,5) The main cause of the urban heat island is the high use of asphalt and concrete in urban environments, which generates a lot of artificial heat, increases detectable heat, and thus increases urban temperatures.(6)

*Corresponding author: e-mail: sunghokil@kangwon.ac.kr
https://doi.org/10.18494/SAM5259

ISSN 0914-4935
https://myukk.org/

Rapid urbanization has accelerated land use and land cover changes, significantly changing the structure and function of urban ecosystems.[7,8] The main problem is that the proliferation of impervious urban surfaces increases heat storage capacity, altering the microclimate and leading to the urban heat island effect. Urban heat island is a phenomenon in which urban areas experience relatively higher temperatures than suburban and rural areas.[6]

Remote sensing techniques are widely employed to study the urban heat island phenomenon, and Landsat imagery is widely used. Landsat images were used to analyze the structural characteristics of the thermal environment in a specific area of Daegu City.[9] Additionally, research has explored the relationship between green space and land surface temperature (*LST*)[10,11] as well as studies on land cover and *LST* using Landsat images.[12] These studies are presented as basic data related to the need to expand green infrastructure and secure green spaces in cities to alleviate the urban heat island effect. We also used Landsat imagery to obtain data at specific points in time and analyzed it through various field surveys and analysis techniques.

However, most land-cover-specific *LST* studies analyze temperature distributions over time or standardize *LST* to compare temperature variations by land cover. This approach overlooks the potential deviations from baseline temperatures specific to different land covers. Therefore, in this study, we aimed to fill this research gap by analyzing relative land surface temperature (*RLST*) across various land covers over multiple time periods. By employing Landsat imagery, we aimed to provide a more nuanced understanding of how different land covers contribute to temperature deviations, ultimately offering insights for urban planning and green infrastructure development.

2. Methods

2.1 Study site

Chuncheon City was selected for this study owing to its relatively stable population and limited recent development, providing a consistent backdrop for analysis. Chuncheon City encompasses a mixture of forest green, urbanized green, and landscape green spaces in the urban area, making it an ideal subject for studying urban green space. The spatial scope of this study is the Chuncheon-si urban area. The total area of Chuncheon City is 1116.83 km^2, the urban area of which is about 333.09 km^2. Chuncheon has an average annual temperature of 11.5 °C, with an average monthly temperature of 25.3 °C in August, the hottest month, and an average monthly temperature of −5 °C in January, the coldest month, with an annual difference of 30.2 °C. In addition, the annual precipitation is 1354.3 mm, with 872.1 mm of precipitation during the summer months of June through August (https://www.chuncheon.go.kr/cityhall/about-chuncheon/introduction/climate/).[13]

2.2 Methods

The temporal scope of this study is based on Landsat 8 images from the years 2014, 2017, and 2020. Specifically, Landsat 8 images were acquired on May 30, 2014, September 19, 2014, May

22, 2017, September 4, 2017, June 15, 2020, and September 19, 2020 (taken at around 11 am). These images were sourced from the United States Geological Survey (USGS, http://earthexplorer.usgs.gov/) and selected only if the cloud cover was less than 10%. The selection of these time periods was guided by the availability of Landsat 8 data starting from 2013 and the aim to analyze data at three-year intervals up to 2021. Additionally, the summer season was chosen because summer worsens the urban heat island effect. However, it was difficult to acquire images in July and August owing to clouds, so images from May to September were used.

We built a GIS database of summer and fall surface temperatures in 2014, 2017, and 2020 for urban areas within the Chuncheon-si district of Gangwon-do. The surface temperature database was divided into urban areas and land cover. For spatial data, *LST* and *RLST* were calculated using the Landsat 8 data provided by the USGS (http://earthexplorer.usgs.gov/) using ArcGIS 10.1 software. In addition, analysis of variance (ANOVA) was performed to verify temperature differences by land cover, and IBM SPSS Statistics version 26 was used as the statistical analysis program. This analysis was conducted to confirm the existence of temperature differences by land cover.

LST can be calculated using Landsat 8's band 10 (thermal infrared band), normalized difference vegetation index (*NDVI*), and normalized vegetation index. The *LST* calculation algorithm shown in Fig. 1 using Landsat 8 satellite images was used as reference.[14]

The *LST* calculation is divided into six steps, and the formula is

$$L_\lambda = M_L \times Q_{cal} + A_L - O_i \,. \tag{1}$$

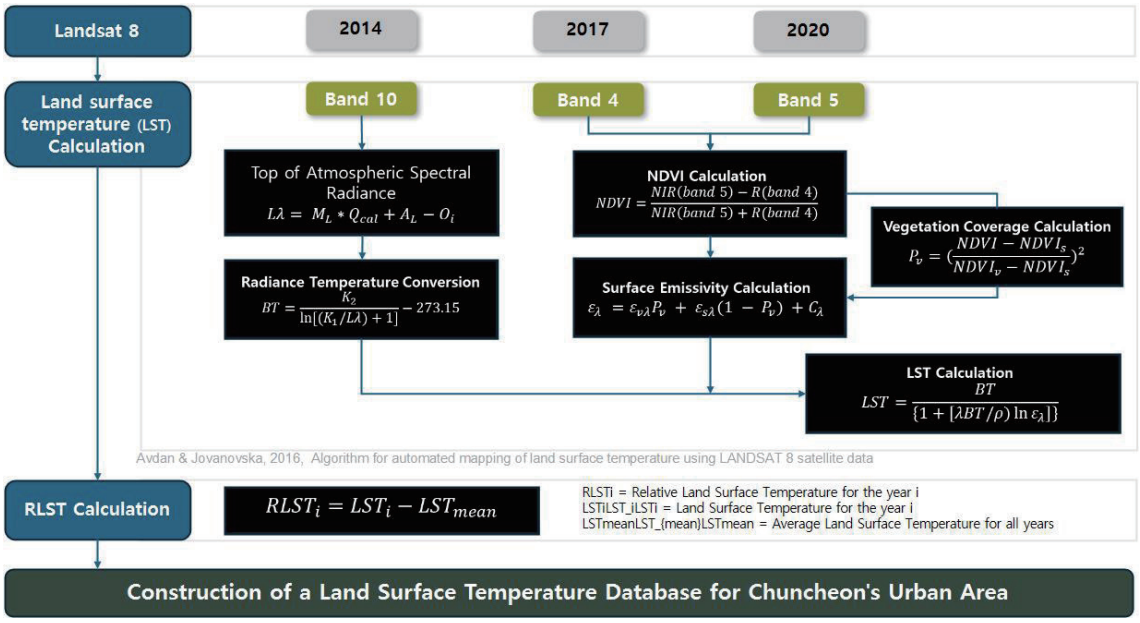

Fig. 1. (Color online) Flowchart of surface temperature calculation in urban area of Chuncheon City.

Here, L_λ is the top of atmospheric spectral radiance, M_L is the specific multiplicative rescaling factor of the band, Q_{cal} is the digital number of the corresponding band, A_L is the specific additive rescaling factor of the band, and O_i is the corrected value of the band.

$$BT = \frac{K2}{\ln\left[\left(\frac{K1}{L\lambda}\right)+1\right]} - 273.15 \tag{2}$$

Equation (2) is used to convert the top-of-atmosphere spectral radiance from Eq. (1) into ℃, where BT is the brightness temperature and $K1$ and $K2$ are the thermal conversion constants for the infrared band of Landsat 8.

$$NDVI = \frac{NIR(Band\,5) - R(Band\,4)}{NIR(Band\,5) - R(Band\,4)} \tag{3}$$

Equation (3) is used to calculate the *NDVI*, where NIR is the near-infrared band (band 5) and R is the red band (band 4).

$$Pv = \left(\frac{NDVI - NDVIs}{NDVIv - NDVIs}\right)^2 \tag{4}$$

Here, Pv is the percentage of vegetation calculated using the *NDVI* in Eq. (3), and *NDVIv* and *NDVIs* are the *NDVI* values for vegetation and soil, respectively (*NDVIv* = 0.5; *NDVIs* = 0.2).

$$\varepsilon_\lambda = \varepsilon_{v\lambda} P_v + \varepsilon_{s\lambda}\left(1 - P_v\right) + C_\lambda \tag{5}$$

Here, ε_λ is the surface emissivity, where ε_v and ε_s are the vegetation and soil emissivities, respectively, and C_λ is the surface roughness (=0.005, which has a value of 0 if the surface is homogeneous and flat).

The emissivity is classified as water if the *NDVI* in Eq. (3) is less than 0, giving it a value of 0.991; as soil if it is between 0 and 0.2, giving it a value of 0.996; as soil and vegetation if it is between 0.2 and 0.5, giving it a value of 0.973; and as vegetation if it is greater than 0.5, giving it a value of 0.973.

$$LST = \frac{BT}{1 + \left[\left(\frac{\lambda BT}{\rho}\right) ln\varepsilon_\lambda\right]} \tag{6}$$

Finally, in Eq. (6), *LST* is the surface temperature in ℃ and BT is the radiation wavelength (λ = 10.895), which has the value of 1.438×10^{-2} m K. *RLST* is then calculated using *LST*, and the

RLST shown in Eq. (7) is the relative surface temperature that represents the change in the thermal environment of the study site considering the weather change and time difference in the remote sensing image.

$$RLSTi = LSTi - LSTmean \tag{7}$$

Here, *LSTi* is the grid value of each year (2014, 2017, or 2020) and *LSTmean* is the average *LST* at the target site in that year. In Eq. (7), if the result is negative (−), the specific area of the study site is considered lower than the average, and if it is positive (+), it is considered higher than the average.

3. Results and Discussion

3.1 *LST* by land cover

On May 30, 2014, the distribution of surface temperature by land cover ranged from 16.7 to 40.3 ℃, and the average surface temperature was 29.0 ℃. On September 19, 2014, the distribution of surface temperature by land cover ranged from 14.9 to 33.3 ℃, and the average surface temperature was 22.6 ℃. On May 22, 2017, the distribution of surface temperature by land cover ranged from 8.5 to 33.7 ℃, and the average surface temperature was 24.2 ℃. On September 4, 2017, the distribution of surface temperature by land cover ranged from 13.6 to 33.4 ℃, and the average surface temperature was 23.8 ℃. On June 15, 2020, the distribution of surface temperature by land cover ranged from 14.7 to 36.7 ℃, and the average surface temperature was 27.1 ℃. On September 19, 2020, the distribution of surface temperature by land cover ranged from 14.4 to 28.6 ℃, and the average surface temperature was 21.0 ℃, as shown in Fig. 2 and Table 1.

Excluding data from September 19, 2014, the average *LST* for each land cover type was in the following order: urban-arid areas > agricultural areas > exposed lands > grasslands > wetlands > forested areas > water bodies. However, in the data from September 19, 2014, the order was different, with tobacco burning, dry areas, agricultural areas, grasslands, pastures, and wetlands, followed by water bodies (20.2 °C) and forest areas (19.2 °C), showing slightly higher temperatures for water bodies. The ANOVA of the *LST* distribution by land cover showed an F value of 364.665, with a significance probability of less than 0.01, indicating a significant difference. This indicates that there is a difference in temperature by land cover.

In particular, the urban-dry areas consistently exhibited the highest surface temperature. On May 30, 2014, these areas had temperatures of 7.2 to 11.3 ℃ higher than the average surface temperature (29.0 ℃). On May 22, 2017, the temperatures were 6.3 ℃ higher than the average surface temperature (24.2 ℃). On September 4, 2017, the temperatures were 10.7 ℃ higher than the average surface temperature (23.8 ℃). On June 15, 2020, the temperatures were 1.9 to 4.1 ℃ higher than the average surface temperature (27.1 ℃). The temperatures were 1.5 to 3.5 ℃ higher than the average surface temperature on September 19, 2020 (21.0 ℃). Urban-dry areas mainly consist of artificial surfaces such as asphalt roads and buildings, where the excessive

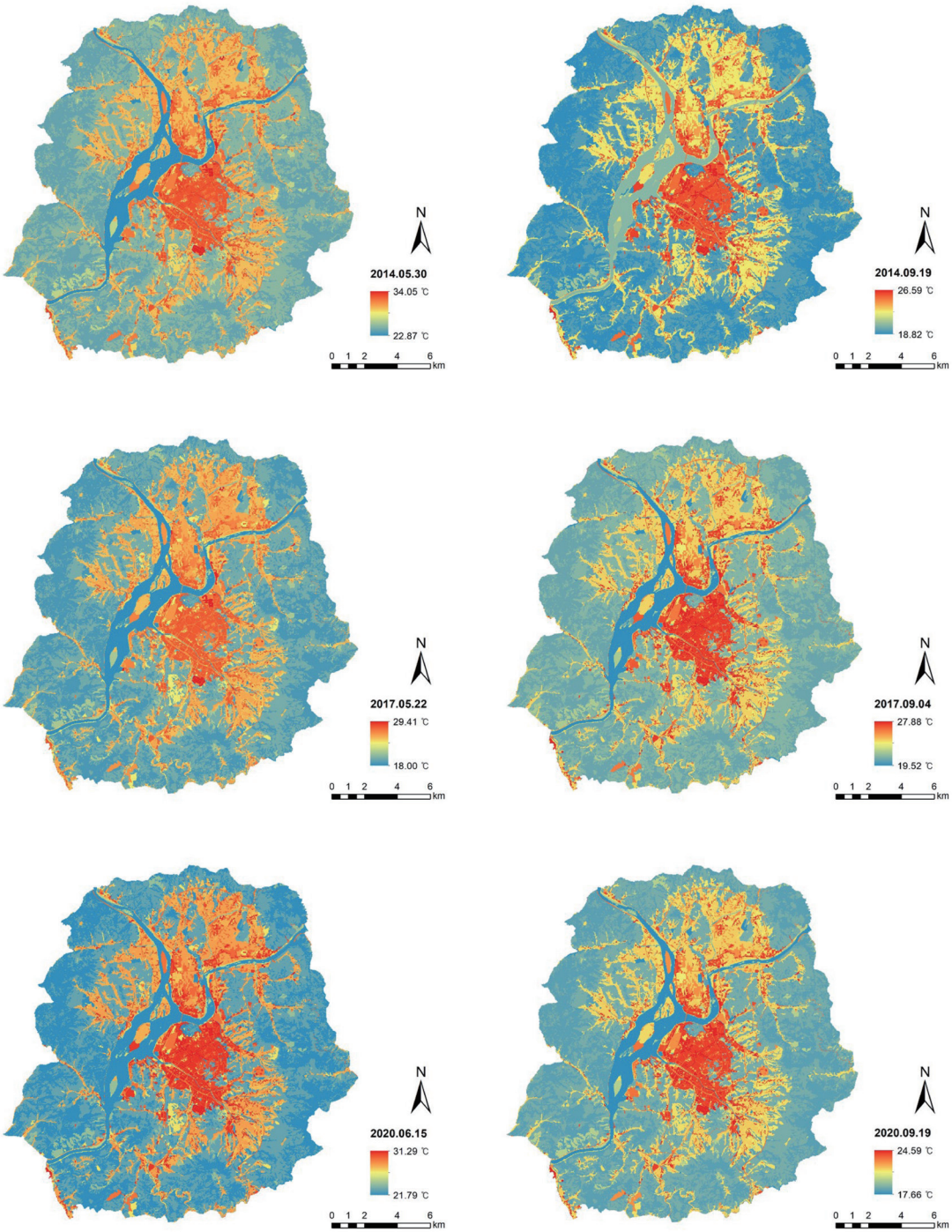

Fig. 2. (Color online) Land surface temperature distribution by land cover (2014, 2017, and 2020).

Table 1
Land surface temperature by land cover (2014, 2017, and 2020).

Level I	Level II	2014/5/30	2017/5/22	2020/6/15
		Mean ± Std	*Mean ± Std*	*Mean ± Std*
Urban-arid land	Residential	32.4 ± 1.9	27.9 ± 2.1	30.3 ± 1.7
	Industrial	34.1 ± 2.4	29.4 ± 2.7	31.3 ± 2.0
	Commercial	32.9 ± 2.0	28.2 ± 2.6	30.7 ± 1.8
	Cultural and recreational	31.4 ± 2.9	26.9 ± 2.5	30.3 ± 2.2
	Transportation	31.3 ± 3.0	26.5 ± 3.4	29.2 ± 2.9
	Public facilities	31.9 ± 2.4	27.2 ± 2.7	30.0 ± 2.3
Agricultural land	Rice paddies	29.6 ± 1.7	25.6 ± 2.2	28.1 ± 1.7
	Fields	29.7 ± 2.3	25.1 ± 2.8	27.8 ± 2.3
	Facility cultivation	30.9 ± 1.5	26.8 ± 2.0	29.4 ± 1.6
	Orchard	29.7 ± 2.1	25.3 ± 2.3	27.4 ± 2.0
	Other planting zones	30.2 ± 2.0	25.7 ± 2.8	28.4 ± 2.0
Forest land	Broadleaf forest	24.1 ± 1.8	18.7 ± 2.2	22.2 ± 1.7
	Coniferous forest	25.1 ± 2.0	19.8 ± 2.4	23.1 ± 2.1
	Mixed forest	25.0 ± 2.0	19.7 ± 2.5	23.0 ± 2.1
Grassland	Natural grassland	26.6 ± 2.9	21.4 ± 3.4	24.3 ± 2.9
	Artificial grassland	28.9 ± 2.6	23.9 ± 3.2	26.8 ± 2.6
Wetland		26.5 ± 2.8	21.5 ± 3.2	24.9 ± 2.7
Bare land	Natural bare land	25.4 ± 3.8	19.4 ± 4.1	23.1 ± 3.4
	Other bare land	31.2 ± 2.7	26.3 ± 3.3	29.1 ± 2.7
Water body		22.9 ± 2.7	18.0 ± 3.1	21.8 ± 2.7

Level I	Level II	2014/9/19	2017/9/4	2020/9/19
		Mean ± Std	*Mean ± Std*	*Mean ± Std*
Urban-arid land	Residential	24.8 ± 1.8	26.5 ± 1.9	23.2 ± 1.7
	Industrial	26.6 ± 2.3	27.9 ± 2.4	24.5 ± 2.2
	Commercial	25.5 ± 1.9	27.1 ± 2.0	23.7 ± 1.7
	Cultural and recreational	25.1 ± 2.4	26.0 ± 2.3	22.5 ± 2.0
	Transportation	24.2 ± 2.4	25.7 ± 2.5	22.5 ± 2.1
	Public facilities	25.0 ± 2.0	26.4 ± 2.1	23.0 ± 1.8
Agricultural land	Rice paddies	22.4 ± 1.3	23.8 ± 1.3	21.2 ± 1.2
	Fields	22.4 ± 1.6	23.7 ± 1.7	21.0 ± 1.4
	Facility cultivation	23.5 ± 1.2	25.1 ± 1.2	22.0 ± 1.0
	Orchard	21.9 ± 1.4	23.3 ± 1.4	20.7 ± 1.2
	Other planting zones	22.8 ± 1.4	24.1 ± 1.4	21.5 ± 1.3
Forest land	Broadleaf forest	18.8 ± 1.3	20.5 ± 1.3	18.2 ± 1.2
	Coniferous forest	19.4 ± 1.4	20.9 ± 1.4	18.6 ± 1.3
	Mixed forest	19.5 ± 1.5	21.1 ± 1.4	18.6 ± 1.3
Grassland	Natural grassland	20.7 ± 2.1	21.8 ± 2.0	19.6 ± 1.5
	Artificial grassland	22.4 ± 2.1	23.6 ± 2.1	20.9 ± 1.8
Wetland		21.4 ± 1.5	22.0 ± 1.8	19.5 ± 1.5
Bare land	Natural bare land	20.8 ± 1.8	21.6 ± 1.9	19.1 ± 1.5
	Other bare land	24.4 ± 2.3	25.4 ± 2.2	22.0 ± 1.9
Water body		20.2 ± 1.5	19.5 ± 2.1	17.7 ± 1.6

energy consumption, high population density, and limited air circulation due to building density contribute to artificial heat release. Therefore, measures such as greening should be urgently implemented to reduce the high land surface temperature in urban-arid areas during summer.

For most of the period, Daewoo Apartment in Gangnam-dong, Deukgye Jugong Apartment in Deukgye-dong, and Seoksa Hyunjin Everville Apartment in Seoksa-dong showed lower land surface temperatures than the single-family residential areas in Hyoja 2-dong and Hupyeong 3-dong. In addition, in Hupyeong 2-dong, where the proportion of residential areas accounts for 71.3% of the total area, the difference between the surface temperature of the specific apartment and that of the single-family house located to the west is distinct, which is likely due to the effect of shadows formed by the apartment and green space. The image from September 19, 2014 showed that cultural and recreational areas had the highest land surface temperatures, followed by industrial and commercial areas. The cultural, physical, and recreational areas are mainly composed of stadiums such as soccer fields and tennis courts, such as Songam Sports Town, Gongjeongcheon Amusement Park soccer field, and lakeside gymnasium outdoor tennis courts. These areas are surfaced with artificial grass, urethane, and other synthetic materials, which are exposed to prolonged solar radiation, resulting in high land surface temperatures.

Commercial areas near the Chuncheon Broadcasting Corporation of the Korea Broadcasting Corporation in Gangnam-dong, commercial areas near Namchuncheon Middle School and Gongjoseon Sculpture Park in Geunhwa-dong, industrial areas located to the north of Dong-myeon, and commercial areas near Gangwon Provincial Office and Onmyo-gil showed lower land surface temperatures than other commercial areas. This appears to be due to the presence of inland water bodies and forested areas that can reduce land surface temperatures.

Industrial and commercial areas have higher average land surface temperatures than other dry and arid areas of land cover types: residential, cultural and recreational, and transportation areas and public facilities. The Deukgye Agricultural and Industrial Complex and Hupyeong General Industrial Complex showed relatively higher land surface temperatures than the surrounding land cover, which is dominated by artificial and impermeable surfaces such as asphalt roads, buildings, and concrete pavers. These areas lack mitigation measures such as green spaces, which could help *LST*. This is believed to be due to a lack of elements.

According to the Land Planning and Utilization Act (Article 77) issued by the Ministry of Land, Infrastructure, and Transport of the Republic of Korea, the building-to-land ratios of industrial and commercial areas are 70 and 90%, respectively. Compared with the building-to-land ratio (70%) of residential areas, there is no significant difference in the presence of asphalt roads, buildings, and facilities. However, industrial and commercial areas tend to emit substantial heat energy due to relatively high energy consumption. The elevated land surface temperatures in these areas are primarily attributed to the lack of green spaces that could otherwise help mitigate heat.

On the other hand, forest lands, grasslands, wetlands, and water areas were 0.1 to 6.1 °C colder than the average surface temperature (29.0 °C) in the data on May 30, 2014 and the average surface temperature (22.6 °C) in the data on September 19, 2014. They were 0.3 to 6.2 °C lower than the average surface temperature (24.2 °C) in the data on May 22, 2017 and the average surface temperature (23.8 °C) in the data on September 4, 2017. Data from June 15, 2020

ranged from 0.3 to 5.3 °C below the average surface temperature (27.1 °C), and data from September 19, 2020 ranged from 0.1 to 3.3 °C below the average surface temperature (21.0 °C). Forested areas had the lowest land surface temperatures for all periods except water bodies. Green space is one of the effective factors in reducing land surface temperature, so greening measures are needed to mitigate the heat island effect in urban and arid areas where land surface temperatures are highest.

In the case of exposed land, temperatures were 2 to 4 ℃ higher than the average temperature around 11 am. This appears to be due to the soil being exposed to solar radiation for a long period, resulting in low soil moisture content and high land surface temperature.[15] Taking the above results together, green space is one of the effective factors in reducing land surface temperature, and greening measures are needed to alleviate the heat island effect in cities and arid areas where land surface temperatures are highest.

3.2 *RLST* by land cover

RLST was analyzed to indicate when a region is below the mean (−) and when it is above the mean (+) [see Eq. (7)]. In the May and June images of 2014, 2017, and 2020, the *RLST* distributions for each land cover ranged from −3.5 to +7.7 °C in 2014, −3.3 to +8.1 °C in 2017, and −2.7 to +6.8 °C in 2020. In the September images from 2014, 2017, and 2020, the *RLST* distributions for each land cover ranged from −1.7 to +6.1 °C in 2014, −2.4 to +6.0 °C in 2017, and −1.8 to +5.1 °C in 2020. Additionally, land covers with positive average *RLST* values in all years included urban-arid land, agricultural land, artificial grasslands, and inland wetlands as shown in Fig. 3 and Table 2.

Despite variations in the distribution of surface temperatures by land cover type across different years, the highest surface temperatures were found in urban-arid areas. Images from May and June in 2014, 2017 and 2020 showed 5.8 to 6.6 °C above the relative land surface temperature (0 °C) in residential areas, 6.8 to 8.1 °C in industrial areas, 6.2 to 6.9 °C in commercial areas, 6.2 to 6.9 °C in cultural areas, 5.0 to 5.8 ℃ in recreation areas, 4.7 to 5.2 ℃ in transportation areas, and 5.5 to 5.9 ℃ in public facilities. Additionally, although the temperature distribution was lower in the September images of 2014, 2017, and 2020, it was 3.8 to 4.6 ℃ higher than the relative land surface temperature (0 ℃) in residential areas, 5.1 to 6. 1 ℃ in industrial areas, and 5.1 to 6.1 ℃ in commercial areas. It was 4.3 to 5.2 °C higher in cultural and recreation areas, 3.0 to 4.6 °C higher in transportation areas, and 3.6 to 4.5 °C higher in public facilities. Among dry and arid regions, industrial regions had the highest *RLST*, and *RLST* has tended to increase since 2017. The ANOVA of the *RLST* distribution by land cover showed an F value of 136.357, with a significance probability of less than 0.01, indicating a significant difference. This indicates that there is a difference in temperature by land cover.

In residential areas, *RLST* was particularly high in areas with a high concentration of single-family homes. In contrast, apartment complexes exhibited relatively lower land surface temperatures, attributed to the shading provided by high-rise buildings and the presence of green spaces within the complex. This suggests that urban planning strategies incorporating high-rise buildings and integrated green spaces can effectively reduce surface temperatures.

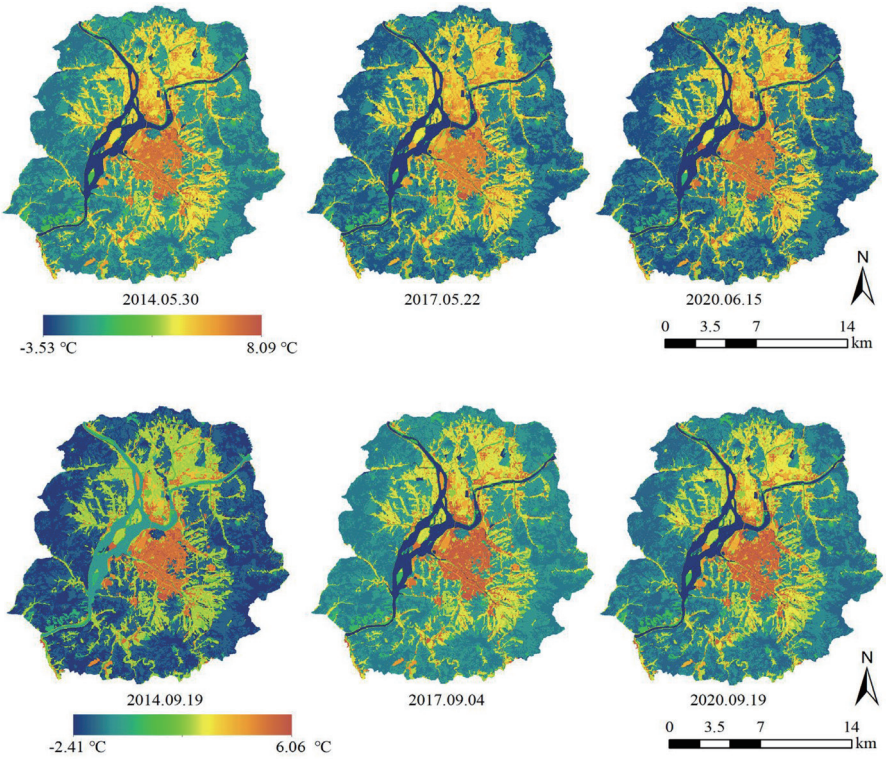

Fig. 3. (Color online) Relative land surface temperature distribution by land cover (2014, 2017, and 2020).

Table 2
Relative land surface temperature by land cover (2014, 2017, and 2020).

Level I	Level II	2014/5/30	2017/5/22	2020/6/15
		Mean ± *Std*	*Mean* ± *Std*	*Mean* ± *Std*
Urban-arid land	Residential	6.0 ± 1.9	6.6 ± 2.1	5.8 ± 1.7
	Industrial	7.7 ± 2.4	8.1 ± 2.7	6.8 ± 2.0
	Commercial	6.5 ± 2.0	6.9 ± 2.6	6.2 ± 1.8
	Cultural and recreational	5.0 ± 2.9	5.5 ± 2.5	5.8 ± 2.2
	Transportation	4.8 ± 3.0	5.2 ± 3.4	4.7 ± 2.9
	Public facilities	5.5 ± 2.4	5.9 ± 2.7	5.5 ± 2.3
Agricultural land	Rice paddies	3.1 ± 1.7	4.3 ± 2.2	3.6 ± 1.7
	Fields	3.3 ± 2.3	3.7 ± 2.8	3.2 ± 2.3
	Facility cultivation	4.4 ± 1.5	5.5 ± 2.0	4.8 ± 1.6
	Orchard	3.3 ± 2.1	3.9 ± 2.3	2.9 ± 2.0
	Other planting zones	3.8 ± 2.0	4.4 ± 2.8	3.9 ± 2.0
Forest land	Broadleaf forest	−2.3 ± 1.8	−2.7 ± 2.2	−2.3 ± 1.7
	Coniferous forest	−1.3 ± 2.0	−1.5 ± 2.4	−1.4 ± 2.1
	Mixed forest	−1.4 ± 2.0	−1.7 ± 2.5	−1.5 ± 2.1
Grassland	Natural grassland	0.2 ± 2.9	0.1 ± 3.4	−0.2 ± 2.9
	Artificial grassland	2.5 ± 2.6	2.5 ± 3.2	2.3 ± 2.6
Wetland		0.1 ± 2.8	0.1 ± 3.2	0.4 ± 2.7
Bare land	Natural bare land	−1.0 ± 3.8	−2.0 ± 4.1	−1.4 ± 3.4
	Other bare land	4.8 ± 2.7	4.9 ± 3.3	4.6 ± 2.7
Water area		−3.5 ± 2.7	−3.3 ± 3.1	−2.7 ± 2.7

Table 2
(Continued) Relative land surface temperature by land cover (2014, 2017, and 2020).

Level I	Level II	2014/9/19	2017/9/4	2020/9/19
		Mean ± *Std*	*Mean* ± *Std*	*Mean* ± *Std*
Urban-arid land	Residential	4.3 ± 1.8	4.6 ± 1.9	3.8 ± 1.7
	Industrial	6.1 ± 2.3	6.0 ± 2.4	5.1 ± 2.2
	Commercial	4.9 ± 1.9	5.2 ± 2.0	4.3 ± 1.7
	Cultural and recreational	4.6 ± 2.4	4.1 ± 2.3	3.0 ± 2.0
	Transportation	3.6 ± 2.4	3.8 ± 2.5	3.1 ± 2.1
	Public facilities	4.4 ± 2.0	4.5 ± 2.1	3.6 ± 1.8
Agricultural land	Rice paddies	1.9 ± 1.3	1.9 ± 1.3	1.7 ± 1.2
	Fields	1.9 ± 1.6	1.8 ± 1.7	1.5 ± 1.4
	Facility cultivation	2.9 ± 1.2	3.2 ± 1.2	2.6 ± 1.0
	Orchard	1.4 ± 1.4	1.4 ± 1.4	1.3 ± 1.2
	Other planting zones	2.3 ± 1.4	2.2 ± 1.4	2.1 ± 1.3
Forest land	Broadleaf forest	−1.7 ± 1.3	−1.5 ± 1.3	−1.3 ± 1.2
	Coniferous forest	−1.1 ± 1.4	−1.0 ± 1.4	−0.8 ± 1.3
	Mixed forest	−1.1 ± 1.5	−0.9 ± 1.4	−0.8 ± 1.3
Grassland	Natural grassland	0.1 ± 2.1	−0.1 ± 2.0	0.2 ± 1.5
	Artificial grassland	1.9 ± 2.1	1.7 ± 2.1	1.5 ± 1.8
Wetland		0.9 ± 1.5	0.1 ± 1.8	0.1 ± 1.5
Bare land	Natural bare land	0.2 ± 1.8	−0.3 ± 1.9	−0.3 ± 1.5
	Other bare land	3.8 ± 2.3	3.5 ± 2.2	2.5 ± 1.9
Water area		−0.4 ± 1.5	−2.4 ± 2.1	−1.8 ± 1.6

Consequently, city planners and policymakers should consider promoting vertical housing developments and enhancing green infrastructure to mitigate the urban heat island effect and improve urban living conditions. These findings underscore the importance of sustainable urban design in addressing climate resilience and promoting environmental health in densely populated areas.

In the May and June images of 2014, 2017, and 2020, land covers with negative mean *RLST* values were forested lands, natural bare lands, and water areas. In particular, water bodies showed *RLST* values that were 2.7 to 3.5 °C lower than the reference land surface temperature (0 °C), forest areas showed land surface temperatures that were 2.3 to 2.7 °C lower than the reference land surface temperature (0 °C), and broadleaf and mixed forests showed land surface temperatures that were 1.4 to 1.7 °C lower than the reference land surface temperature (0 °C). On the other hand, in the September images of 2014, 2017, and 2020, the temperature distribution was lower, but the land covers with negative average *RLST* values were forested areas and water bodies. The *RLST* values of forest lands were −1.3 to −1.7 °C in the case of broadleaf forests, −0.8 to −1.1 °C in the case of mixed forests, −0.8 to −1.1 °C in the case of coniferous forests, and −0.4 to −2.4 °C in the case of water areas.

On the basis of the above results, man-made elements such as asphalt roads and buildings are identified as factors that increase land surface temperature in summer, while natural elements such as green spaces and water bodies are believed to be mitigating factors that reduce land surface temperature. The findings showed that the land surface temperature increases as dense

buildings and barren land increase such as the urban-arid land of land cover types, and the land surface temperature decreases in areas with vegetation.[16] These results demonstrate the effectiveness of natural elements such as green spaces, parks, rivers, plants, and water in improving the microclimate through the absorption of solar heat and cooling through evapotranspiration.[17]

As emphasized in the introduction, the provision of green space is very important for improving urban thermal environments and should be considered alongside ecological efforts that take the urban environment into account.[18] To mitigate the urban heat island effect and improve urban living conditions, it is imperative to expand green spaces through various approaches, including parks, gardens, green infrastructure, and low-impact development.

4. Conclusions

In this study, we utilized Landsat 8 images to extract and analyze land surface temperatures in Chuncheon from 2014 to 2020, with a focus on variations by land cover. By applying *RLST*, the analysis provided a clear understanding of temperature differences across different land cover types.

The findings showed that land surface temperatures are consistently higher in urban-arid and residential areas, primarily due to man-made structures such as asphalt roads and buildings. Industrial areas exhibited the highest *RLST* and an increasing trend since 2017. Within residential areas, densely packed single-family homes showed elevated *RLST*, whereas high-rise apartments showed relatively low land surface temperatures due to shade formation and green space distribution within the complex. Conversely, natural land covers such as local forests, water areas, and natural grasslands showed negative mean *RLST* values, underscoring their cooling effects.

RLST serves as a useful metric for understanding land surface temperature changes relative to a baseline of 0 °C. However, different standardization methods can lead to varying interpretations. Despite this, the *RLST* method simplifies the assessment of temperature states across different land covers.

Our study's reliance on intermediate classification of land cover maps highlights a limitation: the need for high-resolution analysis to capture fine details, as Landsat images do not provide sufficient granularity. Future research should focus on high-resolution land surface temperature analysis for each land cover classification. In addition, to understand the exact temperature variation in the same region, surface temperature changes should be analyzed by time of day (morning, noon, afternoon), which was not possible in this study. In the future, the acquisition of time series data in addition to high-resolution data is worth exploring.

The persistence of the urban heat island effect and the gradual increase in land surface temperature over time underscore the urgent need for sustainable urban ecosystem planning. Policies aimed at expanding both the quantity and quality of green spaces and improving the water environment are essential. Comprehensive urban planning should incorporate strategies to enhance green infrastructure and water bodies, thereby mitigating the urban heat island effect and promoting a more sustainable urban environment.

In conclusion, this study provides valuable insights into the impacts of land cover on land surface temperatures and highlights the importance of integrating green spaces into urban planning to address rising temperatures and improve urban resilience.

Acknowledgments

This study was supported by the Technology Development Project for Creation and Management of Ecosystem-based Carbon Sinks (RS-2023-00218245) through KEITI, Ministry of Environment.

References

1 R. T. Forman: Urban ecology: science of cities (Cambridge University Press, Cambridge, 2014).
2 Ministry of Environment: https://me.go.kr/home/web/policy_data/read.do?menuId=10262&seq=7564 (assessed August 2023).
3 A. J. Arnfield: Int. J. Climatol. **23** (2003) 1. https://doi.org/10.1002/joc.859
4 J. De Blois, T. Kjellstrom, S. Agewall, J. A. Ezekowitz, P. W. Armstrong, and D. Atar: Cardiol. **131** (2015) 209. https://doi.org/10.1159/000398787
5 G. Galea and D. Vlahov: Annu. Rev. Public Health. **26** (2005) 341. https://doi.org/10.1146/annurev.publhealth.26.021304.144708
6 J. A. Voogt, and T.R. Oke: Remote Sens. Environ. **86** (2003) 370. https://doi.org/10.1016/S0034-4257(03)00079-8
7 X. Li, W. Zhou, and Z. Ouyang: Landsc. Urban Plan. **114** (2013) 1. https://doi.org/10.1016/j.landurbplan.2013.02.005
8 W. Zhou, G. Huang, M. L. Cadenasso: Landsc. Urban Plan. **102** (2011) 54. https://doi.org/10.1016/j.landurbplan.2011.03.009
9 S. Eo, H.-S Choi., G. Kim, and G. Lee: J. Climate Change Res. **12** (2021) 713. https://doi.org/10.15531/KSCCR.2021.12.6.713
10 S.-H. Kil, Y. J. Yun. J. For. Environ. Sci. **34** (2018) 246. https://doi.org/10.7747/JFES.2018.34.3.46)
11 P. Yulin, and Y.-H. Kim: J. Assoc. Korean Photo-Geogr. **30** (2020) 126. https://doi.org/10.35149/jakpg.2020.30.4.009
12 H. Y. Kong, S. H. Kim, and H. Cho: Ecol. Resil. Infrastruct. **3** (2016) 315. https://doi.org/10.17820/eri.2016.3.4.315
13 https://www.chuncheon.go.kr/cityhall/about-chuncheon/introduction/climate/ (accessed August 2024).
14 U. Avdan and G. Jovanovska: J. Sensors **1480307** (2016) 1. https://doi.org/10.1155/2016/1480307
15 V. M. Sayão, N. V. dos Santos, W. de Sousa Mendes, K. P. P. Marques, J. L. Safanelli, R. R. Poppiel and J. A. M. Demattê: Geoderma Reg. **22** (2020) e00313. https://doi.org/10.1016/j.geodrs.2020.e00313
16 Q. Sun, Z. Wu, and J. Tan: Environ. Earth Sci. **65** (2012) 1687.
17 A. Aboelata and S. Sodoud: Build Environ. **168** (2020) 106490. https://doi.org/10.1016/j.buildenv.2019.106490
18 S. Meerow, and J. P. Newell: Landsc. Urban Plan. **159** (2017) 62. https://doi.org/10.1016/j.landurbplan.2016.10.005

About the Authors

Young-Jo Yun is an associate professor at Kangwon National University. He graduated from Kangwon National University in 1994, majoring in landscape architecture. He earned his Ph.D. degree from Kangwon National University and his MLA degree from Hongik University. His research interests include landscape design, environmental design, and historical landscape environments. (yyj@kangwon.ac.kr)

Sung-Ho Kil is an associate professor at Kangwon National University. He graduated from Kangwon National University in 2003, majoring in landscape architecture. He earned his MLA and Ph.D. degrees from Seoul National University in 2007 and 2014, respectively. His research interests include ecological restoration, spatial ecology, and landscape ecology.
(sunghokil@kangwon.ac.kr)

Sungmin Lee is an assistant professor in the Department of Landscape Architecture and Urban Planning at Texas A&M University. He earned his bachelor's and master's degrees in landscape architecture from Seoul National University in 2007 and 2009, respectively. He earned his Ph.D. degree in 2018 from Texas A&M University. His primary research interests are in addressing the needs of vulnerable populations, such as older adults, the benefits of green space, and the mitigation of health disparities and environmental inequalities (sungminlee@tamu.edu).